Int. J. Therm. Sci. (2001) 40, 937–948

S1290-0729(01)01280-7/FLA

Series solution of low Dean and Germano number flows in helical rectangular ducts ☆

David L. Thomson, Yildiz Bayazitoglu *, Andrew J. Meade Jr

Department of Mechanical Engineering and Materials Science, William Marsh Rice University, 6100 Main St., Houston, TX 77005-1892, USA

(Received 17 March 2000, accepted 12 January 2001)

Abstract — The flow in a helical duct with rectangular cross-section is analyzed. A series solution based on curvature and torsion is introduced. The components of the series are determined analytically using appropriate eigenfunction expansions. The resulting solution is limited to flows in the low Dean number, low Germano number regime. An analytical friction factor relation is established and compared with previous numerically determined correlations. © 2001 Éditions scientifiques et médicales Elsevier SAS

helical ducts / electromagnetic heating / friction factor / fluid flow

Nomenclature

D_h	hydraulic diameter	m
De	Dean number	
P_H	pitch of the helix	m
R_H	radius of the helix	m
Re	Reynolds number	
U	average velocity in a straight duct	$m{\cdot}s^{-1}$
a	height of cross section	m
b	width of cross section	m
d	coefficient in assumed stream function solution	
h	scale factors of orthogonal curvilinear coordinates	
u	axial velocity component	$m{\cdot}s^{-1}$

Greek symbols

Λ	aspect ratio of rectangular cross section (height/width)	
Φ	angle of the helix	
κ	curvature	
ρ	density	$kg{\cdot}m^{-3}$
τ	torsion	
ϕ	angle of rotation of the cross section coordinate system	
ψ	cross sectional stream function	$m^2{\cdot}s^{-1}$

Subscripts

C	curved duct component
H	helical duct component
S	straight duct component
T	torroidal duct component
W	twisted duct component

Superscripts

$'$	single derivative
$\bar{}$	averaged quantity
$\breve{}$	rescaled quantity
$\hat{}$	unit vector
$\sim$	dimensional quantity

1. INTRODUCTION

During experimental studies on the production of fine metal powders by electromagnetic vaporization, it was found that the cooling of a levitating coil used to produce an alternating magnetic field posed a significant mechanical problem. The coil has a rectangular cross-section to minimize the stacking space while maximizing the levitating effect. The electric current used to levitate an object within the helix causes extreme heating, so

☆ This work is supported by the Texas Advanced Technology Program, Grant No. 003604-041 and by the National Science Foundation, Grant No. CTS-9312379.

* Correspondence and reprints.
E-mail address: bayaz@rice.edu (Y. Bayazitoglu).

cooling fluid is pumped through the coil. The resulting flow rate through such a coil was less than would be expected for a straight duct of the same length.

According to reviews by references [1, 2], curved tubes have higher heat transfer rates and friction factors than equivalent straight ducts. These phenomena are the result of increased mixing caused by the inducement of secondary Dean-type flow due to curvature effects. Torsion due to the non-planarity of a helix may slightly enhance or significantly alter the circulation, depending on its magnitude.

A large number of investigations into ducts with negligible torsion have been completed [1, 2]. The first analytical investigation, flow in a curved duct with a circular cross-section, was performed by Dean [3]. While many of the later studies involved more complicated geometries and extensions to heat transfer characteristics, torsion was either neglected or artificially introduced in an effective radius parameter until more recently. One of the first analytical studies to legitimately include the torsion effect was performed by Wang [4]. His analysis used a non-orthogonal coordinate system that complicated the solution process. Germano [5] introduced an orthogonal coordinate system that has become a standard for later analyses, such as Germano [6], Tuttle [7], and Bolinder [8]. Imposing a rectangular cross-section on such a duct complicates the analysis compared to a circular or elliptical cross-section. Only numerical [8–10] and experimental solutions of flows in helical rectangular ducts are presently available. Note that reference [8] begins an analytical solution of the rectangular duct but determines the actual components by finite volume methods. Only first-order effects of torsion and curvature are included, which do not allow friction factor results to be obtained that are different from straight duct flow. The effect of torsion on heat transfer characteristics, as investigated by Bolinger and Sunden [11], are based on the flow field analysis presented in Bolinger [8, 10].

In this paper the flow through a helical rectangular duct is investigated. A series solution based on curvature and torsion is introduced similar to Germano [5, 6], Tuttle [7], and Bolinder [8]. The components of the series are determined using appropriate analytical eigenfunction expansions. This second-order method, which is extensible to higher orders, allows the analytical prediction of the increased pressure drop of a curved duct. Comparisons are made with full-scale numerical models. The solution is limited to low Dean and Germano number flows and is useful when curvature (toroidal ducts), torsion (twisted ducts), or both (helical ducts) are important.

2. PROBLEM FORMULATION

2.1. General equation of a helix

The duct being considered is a right handed helix as shown in *figure 1*. The centerline of the helix (axis of the duct) is written parametrically using the angle of the helix, Φ, as

$$\boldsymbol{R}(\Phi) = R_{\mathrm{H}}\cos\Phi\hat{\boldsymbol{e}}_X + R_{\mathrm{H}}\sin\Phi\hat{\boldsymbol{e}}_Y + P_{\mathrm{H}}\Phi\hat{\boldsymbol{e}}_Z \qquad (1)$$

where the radius (R_{H}), pitch (P_{H}), and global coordinates (XYZ) are given in *figure 1*, and $\hat{\boldsymbol{e}}$ is a unit direction vector. The arclength is defined as $\mathrm{d}\tilde{s} \equiv (\mathrm{d}\boldsymbol{R}\cdot\mathrm{d}\boldsymbol{R})^{1/2}$, thus

$$\tilde{s} = \Phi\left(R_{\mathrm{H}}^2 + P_{\mathrm{H}}^2\right)^{1/2} \qquad (2)$$

where the tilde signifies a dimensional quantity where needed to avoid ambiguity.

The Frenet formulas for a space curve define the tangent ($\widehat{\boldsymbol{T}} \equiv \boldsymbol{R}'$), normal ($\widehat{\boldsymbol{N}} \equiv \widehat{\boldsymbol{T}}'/\tilde{\kappa}$), and binormal ($\widehat{\boldsymbol{B}} \equiv \widehat{\boldsymbol{T}} \times \widehat{\boldsymbol{N}}$) directions. Here each prime (´) designates a single derivative, the curvature $\tilde{\kappa}$ is defined by the normal, and the torsion is defined as $\widehat{\boldsymbol{B}}' \equiv -\tilde{\tau}\widehat{\boldsymbol{N}}$. In general $\tilde{\kappa} = (\boldsymbol{R}''\cdot\boldsymbol{R}'')^{1/2}$ and $\tilde{\tau} = (\boldsymbol{R}' \times \boldsymbol{R}''\cdot\boldsymbol{R}''')/\tilde{\kappa}^2$. For the regular helix in equation (1),

$$\tilde{\kappa} = R_{\mathrm{H}}/\left(R_{\mathrm{H}}^2 + P_{\mathrm{H}}^2\right) \quad \text{and} \quad \tilde{\tau} = P_{\mathrm{H}}/\left(R_{\mathrm{H}}^2 + P_{\mathrm{H}}^2\right) \quad (3)$$

The Frenet triad can then be rewritten using equations (2) and (3) as

$$\begin{aligned}
\widehat{\boldsymbol{T}} &= \left[\tilde{\kappa}\left(-\sin\Phi\hat{\boldsymbol{e}}_X + \cos\Phi\hat{\boldsymbol{e}}_Y\right) + \tilde{\tau}\hat{\boldsymbol{e}}_Z\right]\left(R_{\mathrm{H}}^2 + P_{\mathrm{H}}^2\right)^{1/2} \\
\widehat{\boldsymbol{N}} &= -\cos\Phi\hat{\boldsymbol{e}}_X - \sin\Phi\hat{\boldsymbol{e}}_Y \\
\widehat{\boldsymbol{B}} &= \left[\tilde{\tau}\left(\sin\Phi\hat{\boldsymbol{e}}_X - \cos\Phi\hat{\boldsymbol{e}}_Y\right) + \tilde{\kappa}\hat{\boldsymbol{e}}_Z\right]\left(R_{\mathrm{H}}^2 + P_{\mathrm{H}}^2\right)^{1/2} \qquad (4)
\end{aligned}$$

For any constant cross-section, the normal and binormal vectors are oriented in the same direction with respect

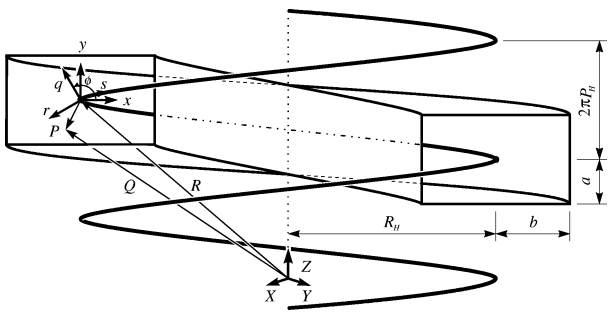

Figure 1. Helical coordinate system.

to the cross-section at any position along the centerline. A discussion on the coordinate system for the duct cross-section can be found in Appendix A.

2.2. Governing equations

Consider laminar incompressible flow through a helical duct of constant cross-section, neglecting buoyancy. These assumptions uncouple the energy equation from the momentum and continuity equations. Assume also that the flow is time independent. The driving force for the flow is a constant axial pressure gradient, $\tilde{p}_{,\tilde{s}}$, where $(\,)_{,\tilde{s}} \equiv \partial/\partial\tilde{s}$. The components of the velocity $\boldsymbol{V}$ in the $\tilde{s}$, $\tilde{q}$, $\tilde{r}$, $\tilde{x}$, and $\tilde{y}$ directions are denoted as $\tilde{u}$, $\tilde{v}_q$, $\tilde{v}_r$, $\tilde{v}_x$, and $\tilde{v}_y$, respectively. The hydraulic diameter is defined based on the height and width ($2a$ and $2b$ of *figure 1*, respectively) of the cross section as $D_\mathrm{h} \equiv 4ab/(a+b)$. The Reynolds, Dean, and Germano numbers are defined with respect to the average of any axial velocity $\tilde{u}_\alpha$ and the viscosity ν as $Re_\alpha \equiv \bar{\tilde{u}}_\alpha D_\mathrm{h}/\nu$, $De_\alpha \equiv \kappa^{\frac{1}{2}} Re_\alpha$, and $Gn_\alpha \equiv \tau Re_\alpha$, respectively, where $\kappa \equiv \tilde{\kappa} D_\mathrm{h}$ and $\tau \equiv \tilde{\tau} D_\mathrm{h}$. All quantities are non-dimensionalized with the characteristic length D_h, the characteristic velocity U (not yet defined), or the characteristic pressure ρU^2, where ρ is the density. The pressure gradient term is defined as $G \equiv -Re\, p_{,s}/\bar{u}_\mathrm{S}$, where $\bar{u}_\mathrm{S}$ is the average velocity in a straight duct. For convenience *Re*, *De*, and *Gn* are assumed to be defined with respect to U except where explicitly noted.

The gradient, divergence, and curl operators based on orthogonal curvilinear coordinates $\boldsymbol{\xi}$, and their scale factors $\boldsymbol{h}$ are presented in Appendix B. The problem is simplified further by considering flow far from either end of the duct. In this region, all terms are assumed axially invariant so that derivatives with respect to s (except pressure) may be neglected. The cross-sectional continuity equation is written in terms of the secondary velocities as

$$\left(\omega^{-1} v_x + \tau y u\right)_{,x} + \left(\omega^{-1} v_y - \tau x u\right)_{,y} = 0$$

where $\omega \equiv 1/(1-\kappa x)$. This suggests a pseudo secondary stream function

$$\begin{aligned} \omega\psi_{,y} &\equiv Re\, v_x + Gn\,\omega y u \quad \text{and} \\ -\omega\psi_{,x} &\equiv Re\, v_y - Gn\,\omega x u \end{aligned} \tag{5}$$

Now applying ψ from equation (5) to the momentum equation in the s direction, we can write

$$\begin{aligned} \omega^{-2}\nabla^2 u = {} & Re\,\omega^{-1} p_{,s} + \omega^{-1} u_{,x}\psi_{,y} - \omega^{-1} u_{,y}\psi_{,x} \\ & - \kappa u\psi_{,y} + \kappa Gn\, y u^2 + Gn\,\omega^{-1} y p_{,x} \\ & - Gn\,\omega^{-1} x p_{,y} - \kappa^2 u + \kappa\omega^{-1} u_{,x} \\ & + 2\kappa\tau Re^{-1}\omega(y\psi_{,xy} - x\psi_{,yy} + \psi_{,x}) \\ & + \tau^2\left(2xyu_{,xy} - 2u - x^2 u_{,yy} - y^2 u_{,xx}\right) \\ & + \tau\nabla^2\psi Re^{-1} + \kappa\tau^2\omega\left(3xyu_{,y} - 2y^2 u_{,x}\right) \\ & - 3\kappa^2\tau^2\omega^2 y^2 u + 3\kappa^2\tau Re^{-1}\omega^2 y\psi_{,y} \end{aligned} \tag{6}$$

where the harmonic and biharmonic operators in the cross-section are $\nabla^2 \equiv \partial^2/\partial x^2 + \partial^2/\partial y^2$ and $\nabla^4 \equiv \nabla^2\nabla^2$. The other momentum equations are combined to get

$$\begin{aligned} \omega^{-1}\nabla^4\psi = {} & \left[(\psi_{,y} - 2\kappa)\partial/\partial x - (\psi_{,x})\partial/\partial y\right] \\ & \times \left[\nabla^2\psi - Gn(yu_{,y} + xu_{,x} + 3u)\right] \\ & + 4Gn\,\omega^{-1}\nabla^2 u \\ & + Gn\,\omega^{-1}\left(x\nabla^2 u_{,x} + y\nabla^2 u_{,y}\right) \\ & + Gn(yu_{,y} - xu_{,x})\psi_{,xy} \\ & + Gn(xu_{,y}\psi_{,xx} - yu_{,x}\psi_{,yy}) \\ & + \kappa Gn\left[3x\nabla^2 u - 2(xu_{,xx} + yu_{,xy} + 2u_{,x})\right] \\ & + 2De\,\omega^{-1} u u_{,y} + \mathrm{O}\left(\kappa^m\tau^n|_{m+n\geqslant 3}\right) \end{aligned} \tag{7}$$

where higher-order terms are lumped together for convenience. After solving equations (6) and (7), the secondary velocities are backed out of equation (5). Equations (6) and (7) are essentially the same governing equations used by references [5–7], and [8]. Defining the cross-sectional aspect ratio as $\Lambda \equiv a/b$ allows the rectangular no-slip boundary conditions to be imposed as

$$\psi_{,x} = 0, \quad \psi_{,y} = 0 \quad \text{and} \quad u = 0 \tag{8}$$

at $x = \pm(1+\Lambda)/4\Lambda$ and $y = \pm(1+\Lambda)/4$.

3. SOLUTION TECHNIQUE

The axial velocity in equation (6) and the pseudo stream function in equation (7) are coupled, complicating a full analytical solution of these partial differential equations. The method of successive approximations, similar to references [4–8], and [12] is used to simplify the analysis. The two nonlinear equations are converted into a series of linearized equations which are solved using known eigenfunction expansions, within the limits of the approximation.

3.1. Decomposition of the governing equations

A loosely coiled and twisted duct with $\kappa, \tau \ll 1$ is considered such that higher-order terms of κ and τ will vanish. Expanding the velocity, stream function, and pressure into a series of increasing integer powers of the curvature and torsion gives

$$\begin{aligned}\chi = \chi_0 &+ \kappa\chi_\kappa + \kappa^2\chi_{\kappa^2} + \cdots \\ &+ \tau\chi_\tau + \kappa\tau\chi_{\kappa\tau} + \kappa^2\tau\chi_{\kappa^2\tau} + \cdots \\ &+ \tau^2\chi_{\tau^2} + \kappa\tau^2\chi_{\kappa\tau^2} + \kappa^2\tau^2\chi_{\kappa^2\tau^2} + \cdots\end{aligned}$$

where χ represents u, ψ, v_x, v_y, and p in turn. The expansions are substituted into the governing equations, and terms with the same powers of κ and τ are collected into separate equations. The first term in each expansion corresponds to flow in a straight duct with the same cross-section, so the zeroth-order cross-flow terms are identically zero.

From the resulting equations, it becomes convenient to rescale higher-order terms with increasing powers of the Reynolds number in a straight duct as

$$\breve{\chi}_{\kappa^m\tau^n} \equiv \chi_{\kappa^m\tau^n}/Re_{\mathrm{S}}^{2m+n}$$

where $\breve{}$ represents a rescaled quantity. This allows all rescaled components to be represented in decreasing Reynolds number notation as

$$\breve{\chi}_{\kappa^m\tau^n} = \breve{\chi}_{\kappa^m\tau_{\mathrm{a}}^n} + Re_{\mathrm{S}}^{-2}\breve{\chi}_{\kappa^m\tau_{\mathrm{b}}^n} + Re_{\mathrm{S}}^{-4}\breve{\chi}_{\kappa^m\tau_{\mathrm{c}}^n} + \cdots$$

so that the individual equations may be solved independently of the Reynolds number.

For convenience all terms are written in the rescaled form from now on and the new notation is neglected. The rescaled expansions may thus be written as

$$\begin{aligned}\chi = \chi_{\mathrm{S}} &+ De_{\mathrm{S}}^2\chi_\kappa + De_{\mathrm{S}}^4\chi_{\kappa^2} + \cdots \\ &+ Gn_{\mathrm{S}}\chi_\tau + De_{\mathrm{S}}^2Gn_{\mathrm{S}}\chi_{\kappa\tau} + De_{\mathrm{S}}^4Gn_{\mathrm{S}}\chi_{\kappa^2\tau} + \cdots \\ &+ Gn_{\mathrm{S}}^2\chi_{\tau^2} + De_{\mathrm{S}}^2Gn_{\mathrm{S}}^2\chi_{\kappa\tau^2} + De_{\mathrm{S}}^4Gn_{\mathrm{S}}^2\chi_{\kappa^2\tau^2} + \cdots\end{aligned}$$

where $u_{\mathrm{S}} = u_0\bar{u}_{\mathrm{S}}$. Higher-order terms must have a decreasing effect on the flow for the series to converge, which is true for low Dean and Germano number flows. Increasing either requires an increased number of terms to accurately approximate the solution.

It becomes convenient to remap the equations into the square $-\frac{1}{2} \leqslant x \leqslant \frac{1}{2}$ and $-\frac{1}{2} \leqslant y \leqslant \frac{1}{2}$. The rescaled biharmonic and harmonic-type operators become

$$\begin{aligned}\breve{\nabla}^4 &\equiv \Lambda^4\frac{\partial^4}{\partial x^4} + 2\Lambda^2\frac{\partial^2}{\partial x^2}\frac{\partial^2}{\partial y^2} + \frac{\partial^4}{\partial y^4} \\ \breve{\nabla}^2 &\equiv \Lambda^2\frac{\partial^2}{\partial x^2} + \frac{\partial^2}{\partial y^2}\end{aligned} \tag{9}$$

The linearized equations are given below, up to second order.

$$\begin{aligned}\psi_0 &\equiv 0 \\ \breve{\nabla}^4\psi_\kappa &= \frac{1}{4}(1+\Lambda)^3u_0u_{0,y} \\ \breve{\nabla}^4\psi_\tau &= -\frac{1}{4}(1+\Lambda)^4G \\ \breve{\nabla}^4\psi_{\kappa_{\mathrm{a}}^2} &= \Lambda\big(\psi_{\kappa,y}\breve{\nabla}^2\psi_{\kappa,x} - \psi_{\kappa,x}\breve{\nabla}^2\psi_{\kappa,y}\big) \\ &\quad + \frac{1}{4}(1+\Lambda)^3(u_0u_{\kappa_{\mathrm{a}},y} + u_{\kappa_{\mathrm{a}}}u_{0,y}) \\ \breve{\nabla}^4\psi_{\kappa_{\mathrm{b}}^2} &= -\Lambda(1+\Lambda)\breve{\nabla}^2\psi_{\kappa,x} \\ &\quad + \frac{1}{4}(1+\Lambda)^3(u_0u_{\kappa_{\mathrm{b}},y} + u_{\kappa_{\mathrm{b}}}u_{0,y}) \\ \breve{\nabla}^4\psi_{\kappa\tau_{\mathrm{a}}} &= \Lambda\big(\psi_{\kappa,y}\breve{\nabla}^2\psi_{\tau,x} - \psi_{\kappa,x}\breve{\nabla}^2\psi_{\tau,y} \\ &\quad + \psi_{\tau,y}\breve{\nabla}^2\psi_{\kappa,x} - \psi_{\tau,x}\breve{\nabla}^2\psi_{\kappa,y}\big) \\ &\quad + \frac{1}{4}(1+\Lambda)^3(u_0u_{\tau,y} + u_\tau u_{0,y}) \\ &\quad - \Lambda\big[1 - \frac{1}{4}(1+\Lambda)^2\big]\big(u_{0,x}\psi_{\kappa,y} - u_{0,y}\psi_{\kappa,x}\big) \\ \breve{\nabla}^4\psi_{\kappa\tau_{\mathrm{b}}} &= \Lambda(1+\Lambda)\bigg\{\bigg[\Lambda^2 + \frac{3}{4}(1+\Lambda)^2\bigg]u_{0,x} \\ &\quad - \breve{\nabla}^2\psi_{\tau,x}\bigg\} \\ &\quad + \bigg[\frac{1}{8}\Lambda(1+\Lambda)^3\bigg]\bigg\{xu_{0,xx} + yu_{0,xy} \\ &\quad - \bigg[1 + \frac{7}{4}\Lambda^{-2}(1+\Lambda)^2\bigg]Gx\bigg\} \\ \breve{\nabla}^4\psi_{\tau^2} &= \Lambda\bigg\{\psi_{\tau,y}\breve{\nabla}^2\psi_{\tau,x} - \psi_{\tau,x}\breve{\nabla}^2\psi_{\tau,y} \\ &\quad - \bigg[1 - \frac{1}{4}(1+\Lambda)^2\bigg](u_{0,x}\psi_{\tau,y} - u_{0,y}\psi_{\tau,x})\bigg\} \\ \breve{\nabla}^2u_0 &= -\frac{1}{4}(1+\Lambda)^2G \\ \breve{\nabla}^2u_{\kappa_{\mathrm{a}}} &= \Lambda(u_{0,x}\psi_{\kappa,y} - u_{0,y}\psi_{\kappa,x}) \\ \breve{\nabla}^2u_{\kappa_{\mathrm{b}}} &= \frac{1}{2}\Lambda(1+\Lambda)u_{0,x} - \frac{1}{8}\Lambda^{-1}(1+\Lambda)^3Gx \\ \breve{\nabla}^2u_\tau &= \Lambda(u_{0,x}\psi_{\tau,y} - u_{0,y}\psi_{\tau,x}) \\ \breve{\nabla}^2u_{\kappa_{\mathrm{a}}^2} &= \Lambda(u_{0,x}\psi_{\kappa_{\mathrm{a}}^2,y} - u_{0,y}\psi_{\kappa_{\mathrm{a}}^2,x})\end{aligned}$$

$$
\begin{aligned}
&\quad + u_{\kappa_a,x}\psi_{\kappa,y} - u_{\kappa_a,y}\psi_{\kappa,x}) \\
\breve{\nabla}^2 u_{\kappa_b^2} &= \Lambda(u_{0,x}\psi_{\kappa_b^2,y} - u_{0,y}\psi_{\kappa_b^2,x} \\
&\quad + u_{\kappa_b,x}\psi_{\kappa,y} - u_{\kappa_b,y}\psi_{\kappa,x}) \\
&\quad + \frac{1}{2}\Lambda(1+\Lambda)\left(u_{\kappa_a,x} - u_0\psi_{\kappa,y} + \Lambda^{-2}x\breve{\nabla}^2 u_{\kappa_a}\right) \\
\breve{\nabla}^2 u_{\kappa_c^2} &= -\frac{1}{16}\Lambda^{-2}(1+\Lambda)^4 G x^2 \\
&\quad + \frac{1}{4}(1+\Lambda)^2(xu_{0,x} - u_0) \\
&\quad + \frac{1}{2}\Lambda(1+\Lambda)u_{\kappa_b,x} \\
\breve{\nabla}^2 u_{\kappa\tau_a} &= \Lambda(u_{0,x}\psi_{\kappa\tau_a,y} - u_{0,y}\psi_{\kappa\tau_a,x} + u_{\kappa_a,x}\psi_{\tau,y} \\
&\quad - u_{\kappa_a,y}\psi_{\tau,x} + u_{\tau,x}\psi_{\kappa,y} - u_{\tau,y}\psi_{\kappa,x}) \\
\breve{\nabla}^2 u_{\kappa\tau_b} &= \Lambda(u_{0,x}\psi_{\kappa\tau_b,y} - u_{0,y}\psi_{\kappa\tau_b,x} \\
&\quad + u_{\kappa_b,x}\psi_{\tau,y} - u_{\kappa_b,y}\psi_{\tau,x}) \\
&\quad + \frac{1}{2}\Lambda(1+\Lambda)\left(u_{\tau,x} - u_0\psi_{\tau,y} + \Lambda^{-2}x\breve{\nabla}^2 u_\tau\right) \\
&\quad + \breve{\nabla}^2\psi_\kappa + x\breve{\nabla}^2\psi_{\kappa,x} + y\breve{\nabla}^2\psi_{\kappa,y} \\
\breve{\nabla}^2 u_{\tau_a^2} &= \Lambda(u_{0,x}\psi_{\tau^2,y} - u_{0,y}\psi_{\tau^2,x} \\
&\quad + u_{\tau,x}\psi_{\tau,y} - u_{\tau,y}\psi_{\tau,x}) \\
\breve{\nabla}^2 u_{\tau_b^2} &= \frac{1}{4}(1+\Lambda)^2\left(xyu_{0,xy} - \Lambda^2 y^2 u_{0,xx} - 2xu_{0,x}\right. \\
&\quad \left. - 2yu_{0,y} - 2u_0 - \Lambda^{-2}x^2 u_{0,yy}\right) \\
&\quad + \frac{1}{16}(1+\Lambda)^4 G\left(\Lambda^{-2}x^2 + y^2\right) \\
&\quad + \breve{\nabla}^2\psi_\tau + x\breve{\nabla}^2\psi_{\tau,x} + y\breve{\nabla}^2\psi_{\tau,y} \qquad (10)
\end{aligned}
$$

The boundary conditions of equation (8) are now imposed at x or $y = \pm\frac{1}{2}$. For many flows of interest, $Re_S^2 \gg 1$ may be assumed without significant loss of accuracy [12]. If this assumption is made the analysis is simplified by eliminating all b and c terms, and the Reynolds number is removed as a direct parameter of the solution. For the results presented within, however, these lower-order terms are included as well.

3.2. Analytical solution of the individual components of the velocity

The velocity through a straight rectangular duct is given by reference [13] as

$$
\begin{aligned}
u_S &= \bar{u}_S \frac{(1+\Lambda)^2 G}{\pi^3} \\
&\quad \times \sum_{k=1,3,5}^{\infty} \frac{(-1)^{(k-1)/2}}{k^3}\left(1 - \frac{\cosh k\pi y/\Lambda}{\cosh k\pi/2\Lambda}\right)\cos k\pi x
\end{aligned} \qquad (11)
$$

Equation (11) is introduced into the dimensionless pressure gradient definition to give

$$
G(\Lambda) = \left[(1+\Lambda)^2\left(\frac{1}{48} - \frac{4\Lambda}{\pi^5}\sum_{k=1,3,5}^{\infty}\frac{\tanh k\pi/2\Lambda}{k^5}\right)\right]^{-1} \qquad (12)
$$

Equation (12) converges rapidly except for large values of Λ. Since this velocity profile is symmetric, in practice $G(\Lambda)$ is found with fewer terms for $\Lambda > 1$ by using $G(\Lambda) = G(1/\Lambda)$.

Biharmonic equations in a square are solved using C and S functions as given by Harris and Reid [14] and Reid and Harris [15]. Harmonic equations in a square are solved using $\cos_k$ and $\sin_k$. A summary of these functions, their properties, and their eigenvalues $(\lambda, \mu, \gamma, \eta)$ are given in *table I*. Note that z, t, and σ are arbitrary functions, coordinates, and eigenvalues; and the superscript iv represents the fourth derivative with respect to t. Each eigenfunction pair defines a complete orthogonal set over the region $-\frac{1}{2} \leqslant t \leqslant \frac{1}{2}$. The solutions of the individual equations are shown below in tensor

TABLE I
Eigenfunctions of the solution ($k = 1 \ldots \infty$).

Eigenfunction	Equation satisfied	Condition(s) at $t = \pm 1/2$	Polarity	Eigenvalue
$C_k(t) = \frac{\cosh\lambda_k t}{\cosh\lambda_k/2} - \frac{\cos\lambda_k t}{\cos\lambda_k/2}$	$z^{iv} = \sigma^4 z(t)$	$z = z' = 0$	Even	$\tanh\lambda_k/2 + \tan\lambda_k/2 = 0$
$S_k(t) = \frac{\sinh\mu_k t}{\sinh\mu_k/2} - \frac{\sin\mu_k t}{\sin\mu_k/2}$	$z^{iv} = \sigma^4 z(t)$	$z = z' = 0$	Odd	$\coth\mu_k/2 - \cot\mu_k/2 = 0$
$\cos_k(t) = \cos\gamma_k t$	$z'' = -\sigma^2 z(t)$	$z = 0$	Even	$\gamma_k = (2k-1)\pi$
$\sin_k(t) = \sin\eta_k t$	$z'' = -\sigma^2 z(t)$	$z = 0$	Odd	$\eta_k = 2k\pi$

notation (repeated indices imply summation). The terms are always even or odd in x and y, so only one set of coefficients, D or d, is required for each term.

$$\begin{aligned}
\psi_\kappa &= (\mathsf{d}_\kappa)_{ij} \boldsymbol{C}_i(x)\boldsymbol{S}_j(y)\\
\psi_\tau &= (\mathsf{d}_\tau)_{ij} \boldsymbol{C}_i(x)\boldsymbol{C}_j(y)\\
\psi_{\kappa_\mathrm{a}^2} &= (\mathsf{d}_{\kappa_\mathrm{a}^2})_{ij} \boldsymbol{S}_i(x)\boldsymbol{S}_j(y)\\
\psi_{\kappa_\mathrm{b}^2} &= (\mathsf{d}_{\kappa_\mathrm{b}^2})_{ij} \boldsymbol{S}_i(x)\boldsymbol{S}_j(y)\\
\psi_{\kappa\tau_\mathrm{a}} &= (\mathsf{d}_{\kappa\tau_\mathrm{a}})_{ij} \boldsymbol{S}_i(x)\boldsymbol{C}_j(y)\\
\psi_{\kappa\tau_\mathrm{b}} &= (\mathsf{d}_{\kappa\tau_\mathrm{b}})_{ij} \boldsymbol{S}_i(x)\boldsymbol{C}_j(y)\\
\psi_{\tau^2} &= (\mathsf{d}_{\tau^2})_{ij} \boldsymbol{S}_i(x)\boldsymbol{S}_j(y)\\
u_0 &= (\mathsf{D}_0)_{ij} \mathbf{cos}_i(x)\,\mathbf{cos}_j(y)\\
u_{\kappa_\mathrm{a}} &= (\mathsf{D}_{\kappa_\mathrm{a}})_{ij} \mathbf{sin}_i(x)\,\mathbf{cos}_j(y)\\
u_{\kappa_\mathrm{b}} &= (\mathsf{D}_{\kappa_\mathrm{b}})_{ij} \mathbf{sin}_i(x)\,\mathbf{cos}_j(y)\\
u_\tau &= (\mathsf{D}_\tau)_{ij} \mathbf{sin}_i(x)\,\mathbf{sin}_j(y)\\
u_{\kappa_\mathrm{a}^2} &= (\mathsf{D}_{\kappa_\mathrm{a}^2})_{ij} \mathbf{cos}_i(x)\,\mathbf{cos}_j(y)\\
u_{\kappa_\mathrm{b}^2} &= (\mathsf{D}_{\kappa_\mathrm{b}^2})_{ij} \mathbf{cos}_i(x)\,\mathbf{cos}_j(y)\\
u_{\kappa_\mathrm{c}^2} &= (\mathsf{D}_{\kappa_\mathrm{c}^2})_{ij} \mathbf{cos}_i(x)\,\mathbf{cos}_j(y)\\
u_{\kappa\tau_\mathrm{a}} &= (\mathsf{D}_{\kappa\tau_\mathrm{a}})_{ij} \mathbf{cos}_i(x)\,\mathbf{sin}_j(y)\\
u_{\kappa\tau_\mathrm{b}} &= (\mathsf{D}_{\kappa\tau_\mathrm{b}})_{ij} \mathbf{cos}_i(x)\,\mathbf{sin}_j(y)\\
u_{\tau_\mathrm{a}^2} &= (\mathsf{D}_{\tau_\mathrm{a}^2})_{ij} \mathbf{cos}_i(x)\,\mathbf{cos}_j(y)\\
u_{\tau_\mathrm{b}^2} &= (\mathsf{D}_{\tau_\mathrm{b}^2})_{ij} \mathbf{cos}_i(x)\,\mathbf{cos}_j(y)
\end{aligned} \tag{13}$$

The solution requires the calculation of the individual constants. The linear operator in equation (10) is applied on the assumed form of the solutions in equation (13). Taking the inner product and integrating over the square forms the operator L and causes the orthogonal terms to drop out. Thus the harmonic operators are of the form

$$\begin{aligned}
\mathsf{L}_{\cos\sin} = {} & \Lambda^2 \left\langle \mathbf{cos}_i'' \,\mathbf{cos}_k \right\rangle \langle \mathbf{sin}_j \,\mathbf{sin}_l \rangle \\
& + \langle \mathbf{cos}_i \,\mathbf{cos}_k \rangle \left\langle \mathbf{sin}_j'' \,\mathbf{sin}_l \right\rangle
\end{aligned} \tag{14}$$

where $\langle z(t)\rangle \equiv \int_{-1/2}^{+1/2} z(t)\,\mathrm{d}t$. These are inverted so that each term is found as

$$\left(L^{-1}_{\cos\sin}\right)_{ijkl} = -4\delta_{ik}\delta_{jl}/\left(\Lambda^2\gamma_i^2 + \eta_j^2\right)$$

where δ is the Kronecker delta. The harmonic coefficients (D) are solved directly. However the biharmonic operators, which are of the form

$$\begin{aligned}
\mathsf{L}_{\mathrm{CS}} = {} & \Lambda^4 \left\langle \boldsymbol{C}_i^{iv} \boldsymbol{C}_k \right\rangle \langle \boldsymbol{S}_j \boldsymbol{S}_l \rangle + 2\Lambda^2 \left\langle \boldsymbol{C}_i'' \boldsymbol{C}_k \right\rangle \left\langle \boldsymbol{S}_j'' \boldsymbol{S}_l \right\rangle \\
& + \langle \boldsymbol{C}_i \boldsymbol{C}_k \rangle \left\langle \boldsymbol{S}_j^{iv} \boldsymbol{S}_l \right\rangle
\end{aligned} \tag{15}$$

have second derivative terms that are not orthogonal to each other. The biharmonic coefficients (d) are coupled due to the coupled inversion of this operator.

The solutions of the first-order coefficients are shown below in tensor notation.

$$\begin{aligned}
(\mathsf{d}_\kappa)_{ij} = {} & \left(\mathsf{L}^{-1}_{\mathrm{CS}}\right)_{ijkl} \frac{1}{4}(1+\Lambda)^3 (\mathsf{D}_0)_{mn} (\mathsf{D}_0)_{op} \\
& \times \langle \mathbf{cos}_m \,\mathbf{cos}_o \,\boldsymbol{C}_k \rangle \left\langle \mathbf{cos}_n \,\mathbf{cos}_p' \,\boldsymbol{S}_l \right\rangle \\
(\mathsf{d}_\tau)_{ij} = {} & \left(\mathsf{L}^{-1}_{\mathrm{CC}}\right)_{ijkl} \left(-\frac{1}{4}\right)(1+\Lambda)^4 G \,\langle \boldsymbol{C}_k \rangle \,\langle \boldsymbol{C}_l \rangle \\
(\mathsf{D}_0)_{ij} = {} & \left(\mathsf{L}^{-1}_{\cos\cos}\right)_{ijkl} \left(-\frac{1}{4}\right)(1+\Lambda)^2 G \,\langle \mathbf{cos}_k \rangle \,\langle \mathbf{cos}_l \rangle \\
(\mathsf{D}_{\kappa_\mathrm{a}})_{ij} = {} & \left(\mathsf{L}^{-1}_{\sin\cos}\right)_{ijkl} \Lambda (\mathsf{D}_0)_{mn} (\mathsf{d}_\kappa)_{op} \\
& \times \left(\left\langle \mathbf{cos}_m' \,\boldsymbol{C}_o \,\mathbf{sin}_k \right\rangle \left\langle \mathbf{cos}_n \,\boldsymbol{S}_p' \,\mathbf{cos}_l \right\rangle \right. \\
& \left. - \left\langle \mathbf{cos}_m \,\boldsymbol{C}_o' \,\mathbf{sin}_k \right\rangle \left\langle \mathbf{cos}_n' \,\boldsymbol{S}_p \,\mathbf{cos}_l \right\rangle \right) \\
(\mathsf{D}_{\kappa_\mathrm{b}})_{ij} = {} & \left(\mathsf{L}^{-1}_{\sin\cos}\right)_{ijkl} \left[\frac{1}{2}\Lambda(1+\Lambda)(\mathsf{D}_0)_{mn} \right. \\
& \times \left\langle \mathbf{cos}_m' \,\mathbf{sin}_k \right\rangle \langle \mathbf{cos}_n \,\mathbf{cos}_l \rangle \\
& \left. - \frac{1}{8}\Lambda^{-1}(1+\Lambda)^3 G \,\langle t\,\mathbf{sin}_k(t) \rangle \,\langle \mathbf{cos}_l \rangle \right] \\
(\mathsf{D}_\tau)_{ij} = {} & \left(\mathsf{L}^{-1}_{\sin\sin}\right)_{ijkl} \Lambda (\mathsf{D}_0)_{mn} (\mathsf{d}_\tau)_{op} \\
& \times \left(\left\langle \mathbf{cos}_m' \,\boldsymbol{C}_o \,\mathbf{sin}_k \right\rangle \left\langle \mathbf{cos}_n \,\boldsymbol{C}_p' \,\mathbf{sin}_l \right\rangle \right. \\
& \left. - \left\langle \mathbf{cos}_m \,\boldsymbol{C}_o' \,\mathbf{sin}_k \right\rangle \left\langle \mathbf{cos}_n' \,\boldsymbol{C}_p \,\mathbf{sin}_l \right\rangle \right)
\end{aligned}$$

The solutions to the second-order coefficients and the analytical integrations required by the solutions are given in reference [12].

Notice that an alternative, two eigenvalue expansion is given in equation (13) for u_0 so that it is of the same form as the higher-order velocity expansions. For a calculation performed to first-order accuracy only, this increases the complexity of the calculation compared to using equation (11). For solutions including second-order terms, the overall complexity is decreased by reducing the number of distinct integrations that need to be calculated. For a practical problem, only consider a finite number of terms $(M \times N)$ in the biharmonic equations (e.g., the first 10×10 eigenvalues) so that the linear operators may be inverted. In this case the four $MN \times MN$ matrices are inverted using a standard LU decomposition/back substitution algorithm similar to that described by Press et al. [16].

Average velocities are determined as $\bar{u}_\alpha = \langle\langle u_\alpha \rangle\rangle$. Only even components contribute to the average, so no first-order change in pressure drop is expected. However,

numerous investigations [1, 2, 17–19] have determined that the pressure drop does increase. A second-order approximation, at least, is required to predict an increase. The average velocity is

$$\bar{u} = 4\sum_{k,l}(-1)^{k+l}\gamma_k^{-1}\gamma_l^{-1} \times \left[\bar{u}_S D_0 + De^4\left(D_{\kappa_a^2} + Re^{-2}D_{\kappa_b^2} + Re^{-4}D_{\kappa_c^2}\right) + Gn^2\left(D_{\tau_a^2} + Re^{-2}D_{\tau_b^2}\right)\right]_{kl} \quad (16)$$

which may be rewritten (up to second order) as

$$\bar{u}_H = \bar{u}_T + \bar{u}_W - \bar{u}_S.$$

4. RESULTS AND DISCUSSION

4.1. Velocity results

Vector and contour plots are shown for secondary and axial velocity components, respectively, for the case $\Lambda = 0.5$ and for various values of *De* and *Gn* in *figure 2* (with $\bar{u}_s = 1$). Note that the outer wall is to the left.

The first-order cross-sectional flow due to curvature is similar to the two cell recirculating pattern determined by Dean [3] for a circular toroidal duct. Centrifugal forces cause the fluid to flow toward the outer wall in the vertical center of the cross-section. In order to satisfy continuity within the cross-section, fluid flows back toward the inside along the upper and lower walls. Near the walls, the difference in boundary conditions (rectangular versus circular) causes the shape to vary from Dean's profile as expected. The first-order components are identical to the results obtained by Bolinder's [8] finite volume solution. Pseudo stream functions of the second-order components are similar to corresponding elliptical results from reference [7] away from the walls, with boundaries producing the expected effects. Note the 'pseudo' stream functions are actual stream functions only for the pure curvature components, as discussed by Bolinder [8].

The second-order curvature components ($\boldsymbol{v}_{\kappa^2}$) push the overall secondary velocity profile toward the outer walls, except at very small *Re*. The distance moved increases for smaller aspect ratios and larger *De*. The larger secondary velocities are concentrated near the outside wall, resulting in increased mixing compared to the inside wall, as seen in *figure 2 (c)* and *(g)*.

At very low *De* and *Gn*, the axial velocity in a helical duct resembles that in a straight duct. At higher *De* the axial velocity profile is shifted toward the outside wall by the secondary flow, as in *figure 2 (d)* and *(h)*. The general effect of τ is to twist the axial velocity profile, as in *figure 2 (f)* and *(h)*. Larger values of *Gn* result in a greater twist.

The average velocities are shown in *table II* for selected cross-sectional aspect ratios. Taking the zeroth and first-order solutions alone, no negative axial velocity contours are predicted for $De < 100$. However, when including the second-order velocity effects as well, some negative contours appear at larger *De* in this range. Obviously the prediction of axial back flow, even in small regions of the cross-section, suggests the need for higher-order solutions in this regime. As an indication of the limiting range of the current solution, the Dean numbers above which an average back flow is predicted are calculated and shown in *table III*. Clearly the notion of an average axial back flow occurring in a flow generated by a favorable pressure gradient is unrealistic. In general the second-order solution is limited to *De* about half of this value or less.

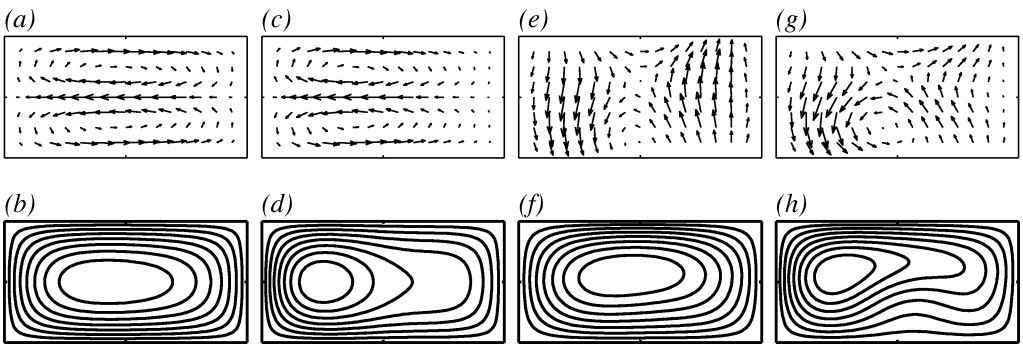

Figure 2. Secondary flow (a, c, e, g) and axial velocity (b, d, f, h), $\Lambda = 0.5$ and $\kappa = 0.1$. (a, b) $De = 20$, $Gn = 0$; (c, d) $De = 35$, $Gn = 0$; (e, f) $De = 20$, $Gn = 50$; (g, h) $De = 35$, $Gn = 50$.

TABLE II
Average axial velocities.

Λ	$\bar{u}_0$	$\bar{u}_{\kappa_a}$	$\bar{u}_{\kappa_b}$	$\bar{u}_{\tau}$	$\bar{u}_{\kappa_a^2}$	$\bar{u}_{\kappa_b^2}$	$\bar{u}_{\kappa_c^2}$	$\bar{u}_{\kappa\tau_a}$	$\bar{u}_{\kappa\tau_b}$	$\bar{u}_{\tau_a^2}$	$\bar{u}_{\tau_b^2}$
1/5	1	0	0	0	−2.10e−9	−1.34e−5	5.89e−1	0	0	−5.93e−8	−1.07e−0
1/2	1	0	0	0	−3.90e−8	−7.51e−5	1.09e−1	0	0	−7.84e−8	−1.72e−1
3/4	1	0	0	0	−1.08e−7	−1.53e−4	5.42e−2	0	0	−3.11e−8	−7.59e−2
1	1	0	0	0	−1.55e−7	−2.21e−4	3.40e−2	0	0	−5.65e−8	−5.63e−2
4/3	1	0	0	0	−1.42e−7	−2.60e−4	2.23e−2	0	0	−3.11e−8	−7.59e−2
2	1	0	0	0	−4.73e−8	−2.06e−4	1.35e−2	0	0	−7.84e−8	−1.72e−1
5	1	0	0	0	−1.17e−9	−5.55e−5	6.85e−3	0	0	−5.93e−8	−1.07e−0

TABLE III
'Stagnation' Dean numbers (solution limited to $De < 0.5De_{\text{stagnation}}$).

	κ	0.001	0.001	0.001	0.01	0.01	0.01	0.1	0.1	0.1
	Gn	250	1000	4000	250	1000	4000	250	1000	4000
Λ										
1/5		147.5	143.4	126.5	146.3	116.9	185.6	88.1	171.4	272.3
1/2		71.0	69.0	57.3	70.6	52.9	84.0	65.4	77.5	123.3
3/4		55.1	54.4	42.2	54.9	49.7	61.9	51.9	57.0	90.8
1		50.4	49.4	37.8	50.1	45.6	55.5	47.6	51.1	81.3
4/3		51.4	50.7	40.3	51.2	45.2	59.1	47.6	54.4	86.6
2		67.7	65.7	55.4	67.1	51.2	81.3	60.3	74.8	119.2
5		170.7	166.6	139.4	169.1	128.6	204.5	87.0	187.2	299.1

4.2. Friction factor results

The Fanning friction factor is defined as

$$f \equiv -(\tilde{p}_{,\tilde{s}} D_h)/\left(2\rho\bar{\tilde{u}}^2\right)$$

The effect of torsion on f is difficult to compare with previous work, but results for toroidal effects are more readily obtainable. Comparisons can be made with reference [17] for a square cross-section and with [18] for a general rectangular cross-section. The ratio of the friction factor of the curved duct compared to a straight duct of the same cross-section is found from the change in flow rates. From equation (16)

$$\frac{(fRe)_C}{(fRe)_S} = \bar{u}_S/\left(\bar{u}_S + De_S^4\left(\bar{u}_{\kappa_a^2} + Re_S^{-2}\bar{u}_{\kappa_b^2} + Re_S^{-4}\bar{u}_{\kappa_c^2}\right) + Gn_S^2\left(\bar{u}_{\tau_a^2} + Re_S^{-2}\bar{u}_{\tau_b^2}\right)\right) \quad (17)$$

where C is a curved duct property and the average velocities are taken from *table II*.

At this point, the choice of the characteristic velocity is discussed. Bolinder [8] defines the characteristic velocity as $U \equiv \nu/D_h$ (which is effectively what is done here and by reference [6] for the secondary velocities only). The disadvantage of this approach is that the Reynolds number does not appear in the governing equations. The average velocity is related back to an artificially defined Reynolds number (and both are defined to be on the order of one). This approach is only successful when the approximation is limited to first-order terms (which do not contribute to the average axial velocity). Most analytical approaches define $U \equiv \bar{\tilde{u}}_S$, which sets the numerator in equation (17) to one, or

$$\frac{(fRe)_C}{(fRe)_S} = 1/\left(1 + De_S^4\left(\bar{u}_{\kappa_a^2} + Re_S^{-2}\bar{u}_{\kappa_b^2} + Re_S^{-4}\bar{u}_{\kappa_c^2}\right) + Gn_S^2\left(\bar{u}_{\tau_a^2} + Re_S^{-2}\bar{u}_{\tau_b^2}\right)\right) \quad (18)$$

Alternatively, the characteristic velocity could be defined as $U \equiv \bar{\tilde{u}}_C$, which sets the denominator in equation (17) to one. Solving the denominator for $\bar{u}_S$ and substituting back gives

$$\frac{(fRe)_C}{(fRe)_S} = 1 - De_S^4\left(\bar{u}_{\kappa_a^2} + Re_S^{-2}\bar{u}_{\kappa_b^2} + Re_S^{-4}\bar{u}_{\kappa_c^2}\right) - Gn_S^2\left(\bar{u}_{\tau_a^2} + Re_S^{-2}\bar{u}_{\tau_b^2}\right) \quad (19)$$

which is equivalent to the first two terms in a series expansion of equation (18). Notice that equations (18)

and (19) both depend on Re_S. Rewrite either, say equation (19), based solely on Re_C to get

$$\frac{(fRe)_C}{(fRe)_S} = 1 - \left[\frac{(fRe)_C}{(fRe)_S}\right]^4 De_C^4 \bar{u}_{\kappa_a^2} - \left[\frac{(fRe)_C}{(fRe)_S}\right]^2 \left(De_C^2 \kappa \bar{u}_{\kappa_b^2} + Gn_C^2 \bar{u}_{\tau_a^2}\right) - \kappa^2 \bar{u}_{\kappa_c^2} - \tau^2 \bar{u}_{\tau_b^2} \quad (20)$$

This requires finding the smallest positive real root of the fourth-order polynomial at every value of Re_C, κ, and τ. Equations (18)–(20) give identical results at very small *Re*. However equation (18) and especially equation (20) diverge more quickly than equation (19), which is used here. Also, equation (20) usually fails to produce any positive real roots for $De > 0.5De_{stagnation}$.

Cheng et al. [18] solved fully-developed rectangular toroidal flow using a finite difference approach. Using the results from multiple runs, varying the curvature and the Reynold's number, they assumed a correlation equation and determined the coefficients using the least square method. Bolinder [17] solved fully-developed square helical flow using a finite volume approach. *Re*, κ, and τ were varied, and a correlation equation based solely on *De* (for small to moderate κ and τ) was obtained.

Figure 3 shows comparisons between the friction factor using the toroidal components of the current numerical solution and Cheng et al. and Bolinder's numerically determined correlations. Note that the symbols in *figure 3*, as well as those in *figures 4* and *5*, do not represent data, but rather indicate the particular value of Λ for each curve. The assumed form of Cheng et al. correlation causes the ratio of the friction factors to become unstable for small *De*. The stable solutions are obtained for limited Dean number intervals. They found that only for helical ducts of small torsion their solution was stable. For larger *De*, their correlation equation is better matched to their actual finite difference solutions. Therefore, for low Dean numbers the current solution provides a better approximation than Cheng et al. correlation. For $De > 0.5De_{stagnation}$, the current solution begins to deviate greatly from Cheng et al. correlation due to the truncation of the series after two terms. Bolinder's correlation (for $\Lambda = 1$) is assumed accurate throughout this region. An increased number of terms in the current solution would allow a Padé approximation of the series, which might lead to accurate friction factor predictions in a larger range of Dean numbers.

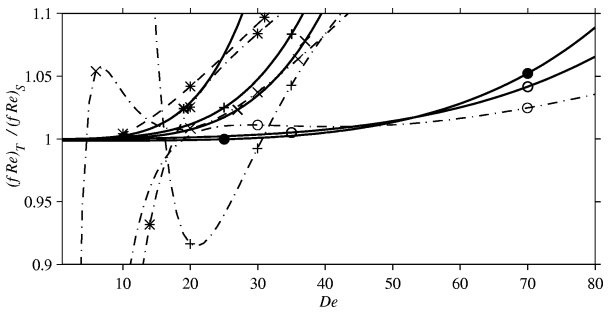

Figure 3. Friction factor ratio of toroidal ducts ($Gn = 0$). Current solution ——, Cheng et al. [18] correlation -·-·-, Bolinder's [8] correlation - - -, $\Lambda = 5$ ∘, $\Lambda = 2$ +, $\Lambda = 1$ ∗, $\Lambda = 0.5$ ×, $\Lambda = 0.2$ •.

Friction factor results for ducts with torsion parameter greater than zero (i.e., true helical ducts) are shown in *figure 4* for several aspect ratios. This figure shows the importance of curvature as a separate parameter (from the Dean number) on the friction factor. This is an indication of the importance of the *b* and *c* terms of the aspect ratio, Λ, in the expansion. For a square cross-section, the effects are small and can be neglected for small values of κ. Bolinder and Cheng et al. did this in their correlations. For large aspect ratios, curvature effects are important at large *De* only. However for small aspect ratios curvature effects are important at small *De* only.

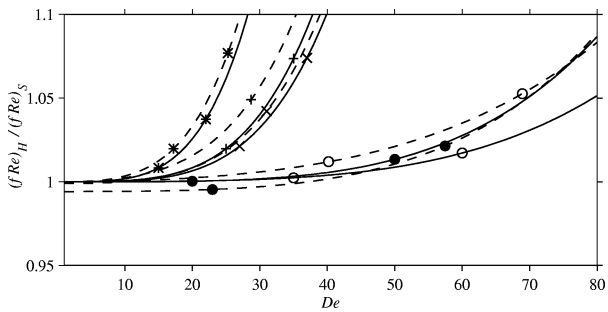

Figure 4. Friction factor ratio of helical ducts ($Gn = 0$). $\kappa = 0.01$ ——, $\kappa = 0.1$ - - -, $\Lambda = 5$ ∘, $\Lambda = 2$ +, $\Lambda = 1$ ∗, $\Lambda = 0.5$ ×, $\Lambda = 0.2$ •.

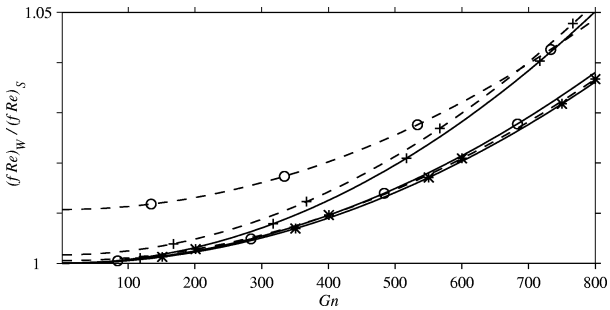

Figure 5. Friction factor ratio of twisted ducts ($De = 0$). $\tau = 0.01$ ——; $\tau = 0.1$ - - -; $\Lambda = 5, 0.2$ ∘; $\Lambda = 2, 0.5$ +; $\Lambda = 1$ ∗.

Friction factor results for twisted ducts are shown in *figure 5*. The importance of torsion as a separate parameter (from the Germano number) is investigated. For a square cross-section with small τ, the friction factor can be approximated as a function of *Gn* only. For ducts with large or small aspect ratios (far from one) τ becomes an important separate parameter at any value of *Gn*.

Helical friction factors are found by combining toroidal and twisted factors as

$$\frac{(fRe)_{\mathrm{H}}}{(fRe)_{\mathrm{S}}} = \frac{(fRe)_{\mathrm{T}}}{(fRe)_{\mathrm{S}}} + \frac{(fRe)_{\mathrm{W}}}{(fRe)_{\mathrm{S}}} - 1 \qquad (21)$$

(for a second-order expansion). As seen in *figures 4* and *5*, the friction factor increases much more quickly with *De* than *Gn*. For 'traditional' helical ducts, τ is at most on the same order of magnitude as $\kappa^{1/2}$ (usually much less), so *De* is much more important than *Gn* in determining the friction factor. Thus, the torsional effects are often ignored entirely when calculating the friction factor for a helical duct.

4.3. Error in eigenfunction series truncation

Tests were performed to estimate the error in the truncation of the eigenfunction expansions. *Figure 6* shows the maximum relative error for a square duct using $M \times M$ coefficients compared to the 'exact' 40×40 coefficient solution. The error decreases as approximately M^{-4} for these cases. For non-square cross-sections, $M \times N$ coefficients are recommended where $N \approx M\Lambda^{1/2}$ and $MN \approx M^2_{\mathrm{square}}$ for the same order of accuracy.

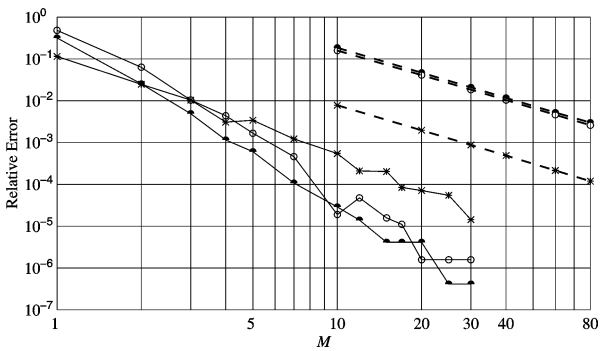

Figure 6. Relative error in solution of velocity components of a square duct ($\Lambda = 1$). PSOR finite difference solution – – – (using an $M+1 \times M+1$ mesh) and eigenfunction solution —— (using $M \times M$ coefficients): u_0 ∗, ψ_κ •, u_{κ_a} ○.

Comparison results are included from a point-successive over-relaxation (PSOR) finite difference solution of the components (similar to Hoffmann and Chiang [20]). A second-order central-difference scheme was used throughout an $(M+1) \times (M+1)$ mesh. The maximum relative error (again compared to the 'exact' 40×40 eigenfunction solution) decreases almost exactly as M^{-2}, as expected. To achieve the same approximate accuracy as a 10×10 eigenfunction expansion, an 801×801 finite difference mesh would be required.

Not only is the eigenfunction solution more accurate than the PSOR solution of the individual terms, it is also easier to calculate. A 10×10 eigenfunction solution requires approximately 4 seconds on a Sparc 10 for a complete second-order solution of all 18 equations. Higher-order solutions only require $O(M^3N + MN^3)$ additional computational steps since the four biharmonic operators, which require $O(M^3N^3)$ steps to invert, are already computed. The time for the finite difference solution, on the other hand, increases significantly since each individual component $(\chi_{\kappa^m\tau_\alpha^n})$ requires an additional solution.

5. CONCLUSIONS

The axially-invariant time-independent laminar flow through curved ducts is calculated using eigenfunction expansions. Analytical forms of the required integrations are given. The rectangular velocity profile is similar to that for an elliptical cross-section (up to second order) except near the boundary where the expected results are obtained.

Since the first-order pressure drop is identically zero, at least a second-order analysis is required to predict the increase in the pressure drop of a curved duct. Analytical forms of the friction factor ratio are given based either on the average velocity in a straight or curved duct. The forms match previous correlations well for low Dean and Germano number flows but deviate at higher Dean and Germano numbers. Higher-order solutions are readily obtainable by the same methods. However since the expansion depends on the Reynolds number, the accuracy cannot be improved indefinitely.

Torsion has little effect on the friction factor for 'traditional' helical ducts but cannot be neglected for more extreme helical or twisted ducts ($\tau \gg \kappa$). Moreover, the velocity profile is significantly altered even at low to moderate values of torsion, though not in an averaged sense. Thus torsion affects the heat transfer characteristics of many helical ducts even when it negligibly affects the friction factor.

REFERENCES

[1] Shah R.K., Joshi S.D., Convective heat transfer in curved ducts, in: Kakac S., Shah R.K., Aung W. (Eds.), Handbook of Single-Phase Convective Heat Transfer, Wiley, New York, 1987, Chapter 5.

[2] Ito H., Flow in curved pipes, JSME Internat. J. 30 (1987) 543–552.

[3] Dean W.R., Note on the motion of fluid in a curved pipe, Phil. Mag. 4 (1927) 208–223.

[4] Wang C.Y., On the low-Reynolds-number flow in a helical pipe, J. Fluid Mech. 108 (1981) 185–194.

[5] Germano M., On the effect of torsion on a helical pipe flow, J. Fluid Mech. 125 (1982) 1–8.

[6] Germano M., The Dean equations extended to a helical pipe flow, J. Fluid Mech. 203 (1989) 289–305.

[7] Tuttle E.R., Laminar flow in twisted pipes, J. Fluid Mech. 219 (1990) 545–570.

[8] Bolinder C.J., First- and higher-order effects of curvature and torsion on the flow in a helical rectangular duct, J. Fluid Mech. 314 (1996) 113–138.

[9] Eason R.M., Bayazitoglu Y., Meade A.J. Jr., Enhancement of heat transfer in square helical ducts, Internat. J. Heat Mass Transfer 37 (1994) 2077–2087.

[10] Bolinder C.J., Numerical visualization of the flow in a helical duct of rectangular cross-section, Experimental and Numerical Flow Visualization ASME 172 (1993) 329–338.

[11] Bolinger C.J., Sunden B., Numerical prediction of laminar flow and forced convection heat transfer in a helical square duct with a finite pitch, Internat. J. Heat Mass Transfer 39 (1996) 3101–3115.

[12] Thomson D.L., Low Dean number flows in helical ducts of rectangular cross section, M.S. thesis, Rice University, Houston, 1996.

[13] Cornish R.J., Flow in pipe of rectangular cross section, Proc. Roy Soc. Sect. A 120 (1928) 691–700.

[14] Harris D.L., Reid, W.H., On orthogonal functions which satisfy four boundary conditions: I. Tables for use in Fourier-type expansions, Astrophys. J. Suppl. Ser. 3 (1958) 429–447.

[15] Reid W.H., Harris D.L., On orthogonal functions which satisfy four boundary conditions: II. Integrals for use with Fourier-type expansions, Astrophys. J. Suppl. Ser 3 (1958) 448–452.

[16] Press W.H., Teukolsky S.A., Vetterling W.T., Flannery B.P., Numerical Recipes in C, Cambridge Univ. Press, New York, 1994.

[17] Bolinder C.J., The effect of torsion on the bifurcation structure of laminar flow in a helical square duct, J. Fluids Engng. 117 (1995) 242–248.

[18] Cheng K.C., Lin R., Ou J., Fully developed laminar flow in curved rectangular channels, J. Fluids Engng. 98 (1976) 41–48.

[19] Thomson D.L., Bayazitoglu Y., Meade A.J., Low Dean number convective heat transfer in helical ducts of rectangular cross section, J. Heat Tran. 120 (1998) 84–91.

[20] Hoffmann K.A., Chiang S.T., Computational Fluid Dynamics for Engineers—Volume I, Engineering Education System, Wichita, 1993.

APPENDIX A: COORDINATE SYSTEM FOR THE DUCT CROSS-SECTION

For any helical duct an appropriate cross-sectional coordinate system must be determined. The intuitive choice is the 'generic' coordinate system used by reference [4]. The magnitudes in the normal and binormal directions are $\tilde{x}$ and $\tilde{y}$. Any position $\boldsymbol{P}$ in the plane of the cross-section can be related to the global origin as $\boldsymbol{Q} = \boldsymbol{R} + \boldsymbol{P}$, or

$$\boldsymbol{Q} = \boldsymbol{R}(\tilde{s}) + \tilde{x}\widehat{\boldsymbol{N}}(\tilde{s}) + \tilde{y}\widehat{\boldsymbol{B}}(\tilde{s})$$

The metric of the generic coordinate system is found by taking the inner product as

$$\begin{aligned} \mathrm{d}\boldsymbol{Q}\cdot\mathrm{d}\boldsymbol{Q} = {} & \mathrm{d}\tilde{x}^2 + \mathrm{d}\tilde{y}^2 \\ & + \mathrm{d}\tilde{s}^2\left(1 - 2\tilde{\kappa}\tilde{x} + \tilde{\kappa}^2\tilde{x}^2 + \tilde{\tau}^2\tilde{x}^2 + \tilde{\tau}^2\tilde{y}^2\right) \\ & - \mathrm{d}\tilde{x}\,\mathrm{d}\tilde{s}(2\tilde{\tau}\tilde{y}) + \mathrm{d}\tilde{y}\,\mathrm{d}\tilde{s}(2\tilde{\tau}\tilde{x}). \end{aligned}$$

It is seen from the cross-terms ($\mathrm{d}\tilde{x}\,\mathrm{d}\tilde{s}$ and $\mathrm{d}\tilde{y}\,\mathrm{d}\tilde{s}$) that this system is non-orthogonal.

To avoid the difficulties inherent in using a non-orthogonal system, consider Germano's [5, 6] helical coordinates. The $\tilde{q}$–$\tilde{r}$ axes rotate through a prescribed angle ($\phi(\tilde{s}) \equiv -\int_0^{\tilde{s}} \tilde{\tau}(\tilde{s}^*)\,\mathrm{d}\tilde{s}^*$) about $\widehat{\boldsymbol{T}}$ as Φ increases. For a helix, $\tilde{\tau}$ is constant and $\phi_0 \equiv 0$, so

$$\phi = -\tilde{\tau}\tilde{s} = -\Phi\, P_{\mathrm{H}}/\left(R_{\mathrm{H}}^2 + P_{\mathrm{H}}^2\right)^{1/2} \qquad \text{(A.1)}$$

Relating any point in the plane normal to $\widehat{\boldsymbol{T}}$ to the global coordinate system gives

$$\begin{aligned} \boldsymbol{Q} = {} & \boldsymbol{R}(\tilde{s}) + \left[\tilde{q}\cos\phi(\tilde{s}) - \tilde{r}\sin\phi(\tilde{s})\right]\widehat{\boldsymbol{N}}(\tilde{s}) \\ & + \left[\tilde{r}\cos\phi(\tilde{s}) + \tilde{q}\sin\phi(\tilde{s})\right]\widehat{\boldsymbol{B}}(\tilde{s}) \end{aligned}$$

which results in the orthogonal metric (evident by the lack of any cross-terms)

$$\mathrm{d}\boldsymbol{Q}\cdot\mathrm{d}\boldsymbol{Q} = \mathrm{d}\tilde{q}^2 + \mathrm{d}\tilde{r}^2 + \mathrm{d}\tilde{s}^2\left(1 - \tilde{\kappa}\tilde{q}\cos\phi + \tilde{\kappa}\tilde{r}\sin\phi\right)^2 \qquad \text{(A.2)}$$

The usual form of the momentum and continuity equations assumes orthogonal curvilinear coordinates. Thus the helical system equation (A.2) is used in this paper.

APPENDIX B: THE GRADIENT, DIVERGENCE, AND CURL OPERATIONS

Let the general curvilinear system (ξ_1, ξ_2, ξ_3) be related to a cartesian system (x, y, z) so that the element of arc length $\mathrm{d}s$ is given by

$$(\mathrm{d}s)^2 = (\mathrm{d}x)^2 + (\mathrm{d}y)^2 + (\mathrm{d}z)^2$$
$$= (h_1\,\mathrm{d}\xi_1)^2 + (h_2\,\mathrm{d}\xi_2)^2 + (h_3\,\mathrm{d}\xi_3)^2$$

which defines the factors h_i. Note that h_i in general will be functions of the new coordinates ξ_i. Then, in the new system, the components of the gradient of a scalar Ψ are

$$\nabla\Psi = \left(\frac{1}{h_1}\frac{\partial\Psi}{\partial\xi_1}, \frac{1}{h_2}\frac{\partial\Psi}{\partial\xi_2}, \frac{1}{h_3}\frac{\partial\Psi}{\partial\xi_3}\right) \tag{B.1}$$

The divergence of any vector $\mathbf{A} = (A_1, A_2, A_3)$ is given by

$$\nabla\cdot\mathbf{A} = \frac{1}{h_1h_2h_3}\left[\frac{\partial}{\partial\xi_1}(h_2h_3A_1), \frac{\partial}{\partial\xi_2}(h_3h_1A_2), \frac{\partial}{\partial\xi_3}(h_1h_2A_3)\right] \tag{B.2}$$

and the components of the vector $\mathbf{B} = \nabla \times \mathbf{A}$ are given by

$$B_1 = \frac{1}{h_2h_3}\left[\frac{\partial}{\partial\xi_2}(h_3A_3) - \frac{\partial}{\partial\xi_3}(h_2A_2)\right] \tag{B.3}$$

with similar expressions for B_2 and B_3.

Equations (B.1)–(B.3) are sufficient to derive the equations of motion in the new coordinate system ξ_i. From the metric of the helical coordinate system of *figure 1*, the following terms apply:

$$\xi_1 = s, \qquad \xi_2 = q, \qquad \xi_3 = r$$
$$h_1 = 1 - \kappa q\cos\phi + \kappa r\sin\phi$$
$$h_2 = 1, \qquad h_3 = 1$$